Deadbeat Model-Predictive Torque Control With Discrete Space-Vector Modulation for PMSM Drives

Yuanlin Wang, *Student Member, IEEE*, Xiaocan Wang, *Member, IEEE*, Wei Xie, *Member, IEEE*, Fengxiang Wang, *Member, IEEE*, Manfeng Dou, *Member, IEEE*, Ralph M. Kennel, *Senior Member, IEEE*, Robert D. Lorenz, *Fellow, IEEE*, and Dieter Gerling, *Member, IEEE*

***Abstract*—This paper proposes an alternative strategy of finite-control-set model-predictive torque control (MPTC) to reduce the computational burden and the torque ripple and decouple the switching frequency from the controller sampling time. An improved discrete space-vector modulation (DSVM) technique is utilized to synthesize a large number of virtual voltage vectors. The deadbeat (DB) technique is used to optimize the voltage vector selection process, avoiding enumerating all the feasible voltage vectors. With this proposed method, only three voltage vectors are tested in each predictive step. Based on the improved DSVM method, the three candidate voltage vectors are calculated by using a novel algebraic way. This new strategy has the benefits of both the MPTC method and the DB method. The effectiveness of the proposed strategy is validated based on a test bench.**

***Index Terms*—Deadbeat (DB), discrete space-vector modulation (DSVM), model-predictive torque control (MPTC), permanent-magnet synchronous machine (PMSM).**

Manuscript received December 15, 2015; revised February 22, 2016, May 11, 2016, July 22, 2016, and October 12, 2016; accepted November 28, 2016. Date of publication January 16, 2017; date of current version April 10, 2017. This work was supported in part by a Chinese Council Scholarship.

Y. Wang and D. Gerling are with the Institute for Electrical Drives and Actuators, Universitaet der Bundeswehr Muenchen, D-85577 Neubiberg, Germany (e-mail: yuanlin.wang@unibw.de; Dieter.Gerling@unibw.de).

X. Wang was with the Institute for Electrical Drive Systems and Power Electronics, Technical University of Munich, 80333 Munich, Germany. She is now with Dong Ming Motor Electric Europe GmbH, 81825 Munich, Germany (e-mail: bubble88.life@gmail.com).

W. Xie was with the Institute for Electrical Drives and Actuators, Universitaet der Bundeswehr Muenchen, D-85577 Neubiberg, Germany. He is now with VOLABO GmbH, 83607 Munich, Germany (e-mail: wei.xie@unibw.de).

F. Wang was with the Institute for Electrical Drive Systems and Power Electronics, Technical University of Munich, 80333 Munich, Germany. He is now with Haixi Institutes, Chinese Academy of Sciences, Jinjiang 362200, China (e-mail: fengxiang.wang@tum.de).

M. Dou is with the School of Automation, Northwestern Polytechnical University, 710072 Xi'an, China (e-mail: doumf@nwpu.edu.cn).

R. M. Kennel is with the Institute for Electrical Drive Systems and Power Electronics, Technical University of Munich, 80333 Munich, Germany (e-mail: ralph.kennel@tum.de).

R. D. Lorenz is with the Wisconsin Electric Machines and Power Electronics Consortium, University of Wisconsin–Madison, Madison, WI 53706 USA (e-mail: lorenz@engr.wisc.edu).

Color versions of one or more of the figures in this paper are available online at http://ieeexplore.ieee.org.

Digital Object Identifier 10.1109/TIE.2017.2652338

I. Introduction

DURING the past decades, finite-control-set model-predictive torque control (FCS-MPTC) [1], [2], also referred to as PTC, has been widely researched and successfully applied to a wide range of drive applications [3]. Compared with continuous-control-set MPTC, although the switching frequency is nonconstant and the switching frequency couples with the sampling frequency [4], FCS-MPTC has its own advantages.

FCS-MPTC exploits the inherent discrete nature of power converters, a modulator is not required, the concept is intuitive and easy to understand, constraints and nonlinearities can be easily included, the resulting controller is easy to implement, etc. [5]–[7]. Additionally, PTC is regarded as an alternative method to direct torque control (DTC). It provides equally fast torque response as DTC, while enabling the consideration of other control goals, such as harmonic distortion, switching frequency, and current protection [1].

In spite of the good features shown above, it has some challenges. On one hand, as all of the feasible voltage vectors are enumerated, resulting in high amount of calculation and long computational time, the sampling frequency and the prediction length are restricted [8], [9]. On the other hand, a single switching state is employed in the entire sampling interval. Thus, a high torque ripple is inevitable compared with modulator-based control methods [10], [11], and the switching frequency couples with the sampling time [4].

To reduce the calculation effort of model-predictive control (MPC), many solutions have been proposed. They can be broadly classified as offline strategies [12], [13] and online strategies [14], [15]. Explicit MPC is proposed in [16], the optimization problem is presolved offline, and the MPC solution turns out to be easy implement. In [17], the optimization problem is solved partially offline. The optimal switch position is found during an online operation by using a binary search tree. However, memory occupation increases with constraints and prediction horizon [4], [18].

In [15], the online generalized predictive control (GPC) is developed to reduce the calculation effort. The optimization of GPC is solved by using a linear and analytical model. However, with this linear GPC, it is very difficult to include system constraints and nonlinearities. In [14], the deadbeat (DB) strategy is used to reduce the number of candidate voltage vectors. Compared with conventional PTC, although calculation load is reduced, large torque ripple still exists.

To reduce the torque ripple of the PTC method, several strategies have been proposed. As the torque ripple and flux linkage ripple are reduced with more available voltage vectors [19]. One of the solutions is to use the complex power circuit topology to generate a large number of voltage vectors, as introduced in [20]–[22]. However, special hardware and a complicate control algorithm are needed, which is not suitable for commonly used applications.

Hysteresis-bound solutions are proposed in [23] and [24], which is developed from DTC. The switching table is replaced by online optimization. In [23], all admissible switching sequences are considered, and the switching frequency is served as an evaluation criterion. However, the switching sequence that minimizes the switching frequency but not minimizes the torque ripple may be selected. Meanwhile, it is difficult to set a proper hysteresis bound [25].

Direct mean torque control is introduced in [24] and [26]. In one sampling period, an active voltage vector is applied first; when the torque reaches the border of the ripple band, the zero-voltage vector is provided to the motor. An improved FCS-MPC is proposed in [27]; the switching point is calculated based on a function, instead of reaching the border. The torque ripple is reduced compared with the conventional PTC method. However, the zero-voltage vector is not the best choice for the second switching state.

An optimal switching point solution is proposed in [11] and [28]. In one sampling period, two consecutive voltage vectors are applied to the motor. The second voltage vector is selected from all of the switching states instead of only the zero-voltage vector. The switching point is achieved by solving an optimization problem. Compared with the conventional PTC method, the torque ripple is reduced. However, as all switching states are enumerated, a large calculation load exists. The modulated MPC (M^2PC) method is proposed in [10]. The second voltage vector is chosen from the two vectors that are adjacent to the first one, instead of all the feasible voltage vectors. With these methods, in one sampling period, only one voltage vector is employed on average, so the improvement is limited.

Discrete space-vector modulation (DSVM) is a promising method for torque ripple reduction. A large number of virtual voltage vectors can be synthesized within a sampling period. In [19] and [29], DSVM is used to improve the drive performance of the basic DTC method. The best voltage vector is selected according to a lookup table. However, with the increase of voltage vectors, new and complex switching tables are required. In addition, it is difficult to define optimal speed ranges for different operation conditions.

DSVM combined with FCS-MPC is proposed in [9] and [30]. The best voltage vector is selected by a cost function; an external modulator is used to output the selected voltage vector. The fatal drawback of this method is that as all of the synthesized voltage vectors are enumerated, the calculation load is much larger than that of basic FCS-MPC. Thus, this method is not suitable for a real control system. Meanwhile, an external modulator is used, which increases the complexity of the control system.

In this paper, the deadbeat-predictive torque control with discrete space-vector modulation (DB-PTC with DSVM) strategy is proposed to reduce the torque ripple and the computation load of the conventional PTC method. An improved DSVM is used to synthesize a large number of virtual voltage vectors in one sampling period. In order to reduce the calculation in voltage vector selection, the deadbeat torque and flux control (DB-DTFC) technique is used. The voltage vector calculated by DB-DTFC is defined as the deadbeat voltage vector (DB-VV). The three feasible voltage vectors that are adjacent to the DB-VV are served as candidates. And the best one is selected by the cost function. The three candidate voltage vectors are calculated by using a new and easy implementation way; an external modulator or a lookup table is not required.

This paper is organized as follows. Section I introduces the background of this paper; the mathematical models of an inverter and a permanent-magnet synchronous machine (PMSM) are given in Section II. In order to overcome the defects of conventional PTC, the DB-PTC with DSVM strategy is proposed in Section III. In Section IV, the implementation of the proposed technique is given. In Section V, the experimental results are shown. This paper is concluded in Section VI.

II. Discrete Models of an Inverter and a PMSM

In this paper, a two level three-phase standard voltage-source inverter (VSI) is used. Eight feasible voltage vectors can be generated by the inverter, as described in the following equation:

$$V_j = \frac{2}{3}u_{\mathrm{dc}}(S_1 + aS_2 + a^2 S_3) \tag{1}$$

where $j = 0, \ldots, 7$ represent the available voltage vectors, $S_x (x = 1, 2, 3)$ denote the switching states of the three inverter legs, and $a = e^{i2\pi/3}$.

In order to predict the future state of the motor, a discrete-time model of the PMSM is developed by using a normal forward Euler approximation equation[14]. Omitting the tedious derivation process, a standard discrete model of the PMSM in the dq frame is described as follows [31]:

$$i_s(k+1) = A_e i_s(k) + B_e u_s(k) + C_e \tag{2}$$

$$\psi_s(k+1) = \psi_s(k) + [u_s(k) - R_s i_s(k) + \omega(k) D_e] T_s \tag{3}$$

$$T_e(k) = \frac{3}{2} p(\psi_{\mathrm{PM}} i_q(k) + (L_d - L_q) i_d(k) i_q(k)) \tag{4}$$

where $i_s = [i_d, i_q]^T$, $u_s = [u_d, u_q]^T$, $\psi_s = [\psi_d, \psi_q]^T$, $C_e = [0, -\psi_{\mathrm{PM}} T_s \omega(k)/L_q]^T$, $D_e = [\psi_q, -\psi_d]^T$, and

$$A_e = \begin{bmatrix} 1 - \dfrac{R_s T_s}{L_d} & \dfrac{L_q T_s \omega(k)}{L_d} \\ -\dfrac{L_d T_s \omega(k)}{L_q} & 1 - \dfrac{R_s T_s}{L_q} \end{bmatrix}, \qquad B_e = \begin{bmatrix} \dfrac{T_s}{L_d} & 0 \\ 0 & \dfrac{T_s}{L_q} \end{bmatrix}$$

where R_s is the stator resistance, T_s is the sampling period, ω is the electrical rotor speed, p is the number of pole pairs, T_e is the electromagnetic torque, θ is the electrical rotor angle, ψ_{PM} is the

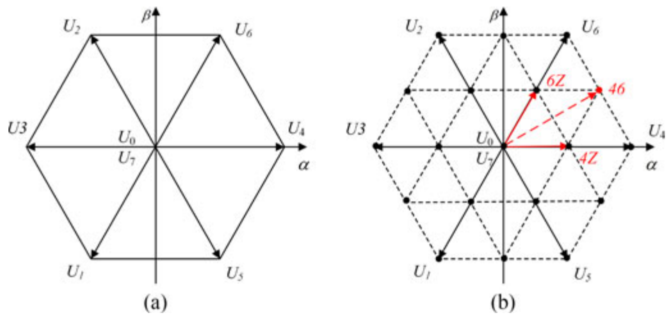

Fig. 1. (a) Basic voltage vectors. (b) Synthesized voltage vectors.

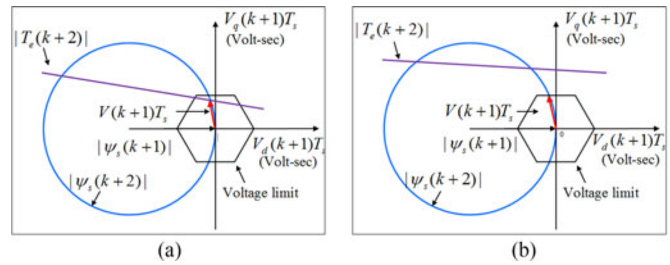

Fig. 2. Graphical solution of DB-VV calculation. (a) DB-VV within the voltage limits. (b) Torque line exceeds the voltage limit.

PM flux linkage, L_d and L_q are stator inductances, u_d and u_q are stator voltages, u_{dc} is the dc-link voltage, i_d and i_q are stator currents, and ψ_d and ψ_q are stator flux linkages.

III. DB-PTC With DSVM Strategy

A. Virtual Voltage Vectors Syntheses

According to the principle of DSVM, in each sampling period, virtual voltage vectors can be synthesized by applying several voltage vectors for prefixed time intervals [19]. For a two-level three-phase standard VSI, if one sampling period is subdivided into N parts equally, the expression of the virtual voltage vectors v^{vir} is shown as (5). The number of feasible voltage vectors (including basic voltage vectors and virtual voltage vectors) is shown as (6)

$$v^{\mathrm{vir}} = \sum_{j=1,2,\ldots,N} t_j V_j^{\mathrm{real}} \tag{5}$$

where

$$\begin{aligned} V_j^{\mathrm{real}} &\in \{V_0, V_1, \ldots, V_7\} \\ t_j &= \frac{T_s}{N} \\ n_{\mathrm{total}} &= 3N^2 + 3N + 2. \end{aligned} \tag{6}$$

The basic voltage vectors are shown in Fig. 1(a); if one sampling period is subdivided into two equal time intervals, 20 voltage vectors can be synthesized, as shown in Fig. 1(b), where the black dots represent the ends of the synthesized voltage vectors. The label "46" represents the voltage vector that is synthesized by U_4 and U_6, and the label "4Z" denotes the voltage vector that is synthesized by U_4 and zero-voltage vector (U_0 or U_7); each one is applied for half of the sampling period.

If all the voltage vectors are enumerated, the amount of calculation load is huge, and it is not suitable for a real control system. Therefore, the computational load must be reduced.

B. Computational Load Reduction

To reduce the calculation amount, the DB-DTFC technique is adopted. The DB-DTFC technique is an inverse-model-based solution. The desired DB-VV is calculated based on the reference torque and the flux linkage. The solution of the DB-VV is developed as follows [32]. The torque change from time instant $t(k+1)$ to $t(k+2)$ can be expressed as

$$\triangle T_e(k+1) = T_e(k+2) - T_e(k+1). \tag{7}$$

The relationship between the desired voltage vector DB-VV$(k+1)$ and the torque change $\triangle T_e(k+1)$ can be expressed as (8). $V_d(k+1)$ and $V_q(k+1)$ are the components of DB-VV$(k+1)$ in d- and q-axes

$$V_q(k+1)T_s = MV_d(k+1)T_s + B \tag{8}$$

where

$$\begin{aligned} M &= \frac{(L_q - L_d)\psi_q(k+1)}{(L_d - L_q)\psi_d(k+1) + L_q\psi_{\mathrm{PM}}} \\ B &= \frac{L_d Lq}{(L_d - L_q)\psi_d(k+1) + L_q\psi_{\mathrm{PM}}}\Bigg[\frac{4\triangle T_e(k+1)}{3p} \\ &\quad - \frac{\omega T_s}{L_d L_q}((L_q - L_d)(\psi_d^2(k+1) - \psi_q^2(k+1)) \\ &\quad - L_q\psi_d(k+1)\psi_{\mathrm{PM}}) \\ &\quad - \frac{R_s T_s \psi_q(k+1)}{L_d^2 L_q^2}((L_q^2 - L_d^2)\psi_d(k+1) - L_q^2\psi_{\mathrm{PM}})\Bigg]. \end{aligned}$$

The graphical solution of DB-DTFC is shown in Fig. 2. In the synchronous volt–second plane, the torque equation is represented by a line. All the voltage vectors on the line can yield the desired torque change $\triangle T_e(k+1)$.

Neglect the stator resistance term, and decouple the cross-coupling term of the stator flux linkage in (3). Then, the flux linkage equation is approximated as

$$\psi_s(k+1) = \psi_s(k) + u_s(k)T_s. \tag{9}$$

For a constant stator flux linkage magnitude, the stator flux linkage is given as

$$\begin{aligned} \psi_s^2(k+2) &= \psi_d^2(k+2) + \psi_d^2(k+2) \\ &= (\psi_d(k+1) + V_d(k+1)T_s)^2 \\ &\quad + (\psi_q(k+1) + V_q(k+1)T_s)^2. \end{aligned} \tag{10}$$

In Fig. 2, flux linkage equation (10) is represented by a circle. The coordinate of circle origin is $[-\psi_d(k+1), -\psi_q(k+1)]$, and the radius is $|\psi_s(k+2)|$. The intersection of torque line and the flux linkage circle is the desired voltage vector (volt–sec) that satisfies both torque and flux linkage requirements.

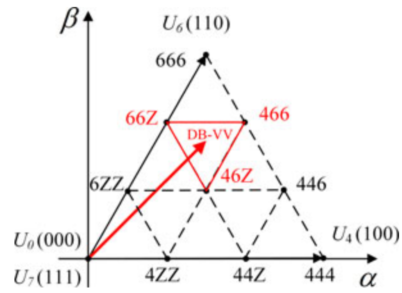

Fig. 3. DB-VV is used to optimize the voltage vector selection process.

The hexagon represents the voltage limit of the inverter. Assume that sufficient voltage is available, such that the intersection falls inside of the hexagon, as shown in Fig. 2(a).

When the torque line exceeds the voltage limit, the voltage vector that maintains the flux linkage command while developing the maximum torque is selected [33]. The graphical solution is shown in Fig. 2(b). This method has the advantage of maintaining desired flux linkage; at the same time, torque reference has been taken into account.

C. DB-PTC With DSVM Strategy

As mentioned above, the DSVM strategy synthesizes a large number of virtual voltage vectors during one sampling period. The DB-VV is the desired voltage vector to achieve reference torque and flux linkage. Therefore, the three voltage vectors that are adjacent to the DB-VV are the optimal candidate voltage vectors for predictive torque and flux control.

For example, as shown in Fig. 3, one sampling period is subdivided into three parts. The three voltage vectors adjacent to the DB-VV are "66Z," "46Z," and "466." In the DB-PTC with DSVM strategy, these three voltage vectors are served as candidates; then, the cost function is used to select the most appropriate one. In this paper, the cost function is shown as (11)

$$\begin{aligned} g(V_j) = \; & \frac{1}{T_{\text{nom}}^2}|T_{\text{ref}} - T_e(k+2)_j|^2 \\ & + \frac{Q_1}{\psi_{\text{nom}}^2}|\psi_{\text{ref}} - |\psi_s(k+2)_j||^2 \\ & + Q_2 S(k+2)_j + I_{\max}(k+2)_j \end{aligned} \tag{11}$$

$$V_{\text{best}} = \underset{j=1,2,3}{\operatorname{argmin}}\, g(V_j) \tag{12}$$

where $j = 1, 2, 3$ represent the three candidate voltage vectors. $S(k+2)_j$ is the switching number of the inverter, and T_{nom} and ψ_{nom} are the rated torque and the flux, respectively.

The precision of torque and the precision of flux are primary goals that must be achieved in order to provide a proper system behavior. Switching frequency is a secondary requirement that is used to improve the system performance [34].

Torque and flux are controlled simultaneously with equal importance. In order to compensate their different nature, torque error and flux error are normalized. Weighting factors Q_1 and Q_2 are selected by the experiment, as shown in Section V-A.

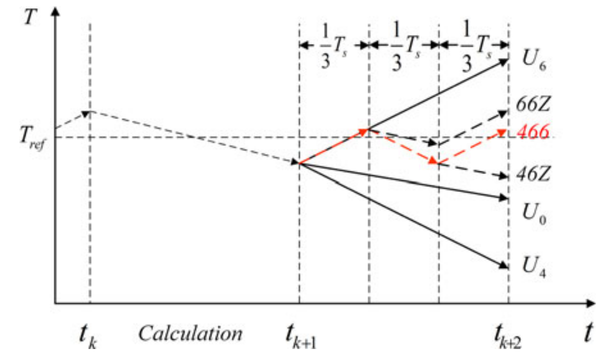

Fig. 4. Torque ripple comparison of the conventional PTC method and the DB-PTC with DSVM strategy.

Current $I_{\max}(k+2)_j$ is taken into account as a protection term [14], [35], [36]. If the current is lower than the current limit, $I_{\max}(k+2)_j$ has no influence on the voltage vector selection. Otherwise, the voltage vector j will be ignored. If the currents generated by all the three voltage vectors exceed the current limit, the zero-voltage vector will be used

$$I_{\max}(k+2)_j = \begin{cases} 0, & |i_s(k+2)_j| \le |i_{s\_\max}| \\ \infty, & |i_s(k+2)_j| > |i_{s\_\max}| \end{cases} \tag{13}$$

where $|i_s(k+2)_j| = \sqrt{i_d^2(k+2)_j + i_q^2(k+2)_j}$.

D. Principle of Torque Ripple Reduction

Compared with the conventional PTC technique, the torque ripple of the proposed DB-PTC with DSVM strategy is lower. The torque ripple reduction principle is analyzed as follows. The relationship between the applied voltage vector and the corresponding torque variation is shown as follows [37]:

$$\frac{dT_e}{dt} = \frac{p}{L_s}\psi_{\text{ss}} \times u_{\text{ss}} + p u_{\text{ss}} \times i_{\text{ss}} - \frac{R_s}{L_s}T_e - \frac{p}{L_s}\psi_{\text{ss}} \times \frac{d}{dt}\psi_r \tag{14}$$

where $u_{\text{ss}} = [u_\alpha, u_\beta]^T$, $i_{\text{ss}} = [i_\alpha, i_\beta]^T$, $\psi_{\text{ss}} = [\psi_\alpha, \psi_\beta]^T$, and $\psi_r = [\psi_r \cos(\theta), \psi_r \sin(\theta)]^T$. In one sampling period, the variation of inductance, flux linkage, and resistance can be ignored. Therefore, for a given voltage vector, the average change of torque over time is approximately linear.

Taking the DB-VV in Fig. 3 as an example, with the conventional PTC method, the best voltage vector will be selected from U_4, U_6, and the zero-voltage vector [14]. In the DB-PTC with DSVM strategy, "66Z," "46Z," and "466" are served as candidate voltage vectors. If all the six voltage vectors are provided to the motor at time instant t_{k+1}, the schematic diagram of torque variations is shown in Fig. 4. It is clear that, at time instant t_{k+2}, the torque ripple produced by "466" is the smallest.

IV. Implementation of DB-PTC With DSVM

A. Improved DSVM Technique

Generally, the synthesized voltage vectors are stored in a lookup table [9],[19]. However, with the increase of voltage vectors, more complex tables are required [19]. To avoid this

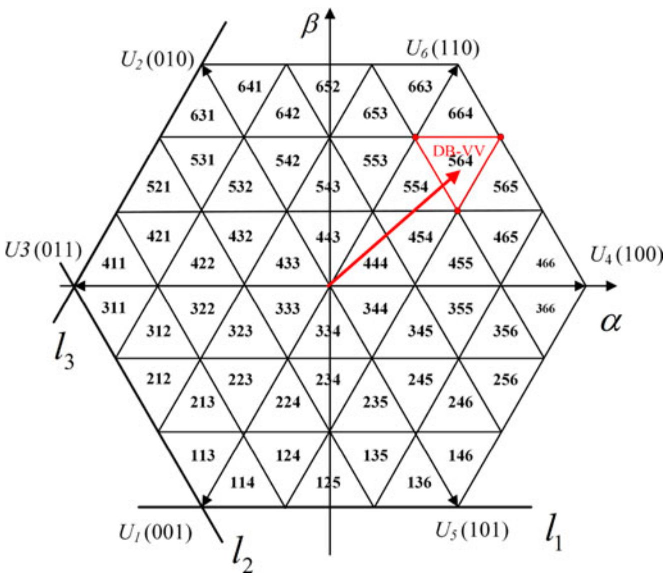

Fig. 5. Triangle contains the end of the DB-VV.

problem, this paper proposes a simple and efficient algebraic solution to calculate the candidate voltage vectors.

Assume one sampling period is subdivided into N parts. l_1, l_2, and l_3 are the three borders of the voltage limit, as shown in Fig. 5. The end point of the DB-VV is (u_α, u_β); the distances from (u_α, u_β) to l_1, l_2, and l_3 is denoted as d_1, d_2, and d_3, respectively, as described in the following equation:

$$\begin{cases} d_1 = |3u_\beta + \sqrt{3}u_{\mathrm{dc}}|/3 \\ d_2 = |3\sqrt{3}u_\alpha + 3u_\beta + 2\sqrt{3}u_{\mathrm{dc}}|/6 \\ d_3 = |3\sqrt{3}u_\alpha - 3u_\beta + 2\sqrt{3}u_{\mathrm{dc}}|/6. \end{cases} \quad (15)$$

Multiplying d_1, d_2, and d_3 with $\sqrt{3}N/u_{\mathrm{dc}}$, and then rounding up, the results are denoted as h_1, h_2, h_3. The triangle that contains (u_α, u_β) can be represented by h, as follows:

$$h = 100h_1 + 10h_2 + h_3. \quad (16)$$

For example, as shown in Fig. 5, if one sampling period is subdivided into three parts equally, the triangle that contains the end of DB-VV is "564."

Candidate voltage vectors are the three apexes of the triangle "564," i.e., $V(1)$, $V(2)$, $V(3)$, which can be figured out according to (17) and (18). In the equation of $V(3)$, if N is an odd number, when h_1 and $h_2 + h_3$ have the same parity, "+" is used; otherwise, "−" is used. If N is an even number, when h_1 and $h_2 + h_3$ have the same parity, "−" is used; otherwise, "+" is used

$$\begin{cases} a = (h_2 + h_3 - 2N)u_{\mathrm{dc}}/(3N) \\ b = \sqrt{3}(h_2 - h_3)u_{\mathrm{dc}}/(3N) \end{cases} \quad (17)$$

$$\begin{cases} V(1) = a + jb \\ V(2) = a - 2u_{\mathrm{dc}}/(3N) + jb \\ V(3) = a - u_{\mathrm{dc}}/(3N) + j(b \pm \sqrt{3}u_{\mathrm{dc}}/(3N)). \end{cases} \quad (18)$$

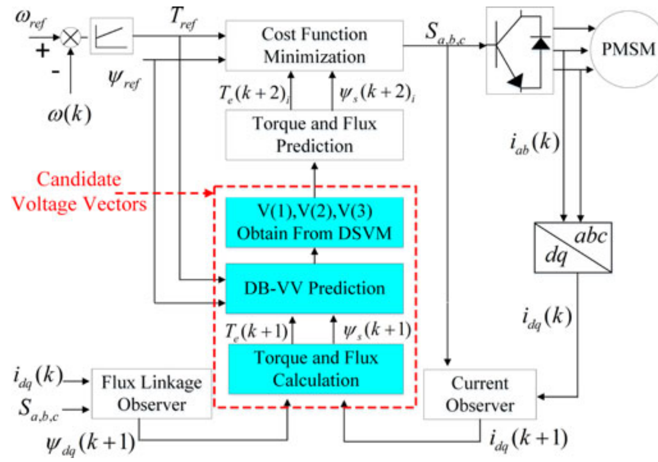

Fig. 6. Control block diagram of the DB-PTC with DSVM technique.

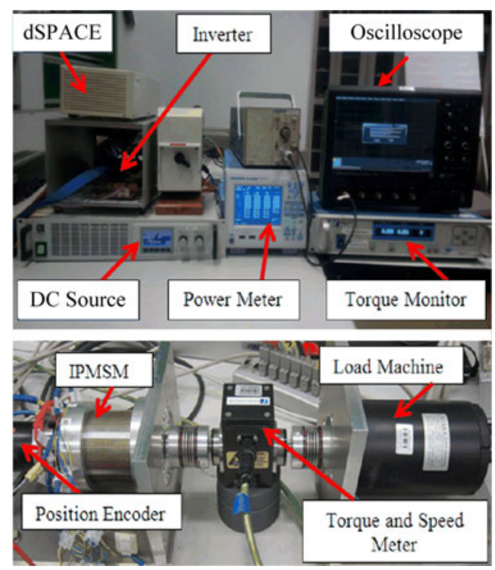

Fig. 7. Test bench used in this experiment.

B. Implementation Process

The control block diagram of the DB-PTC with DSVM method is shown in Fig. 6. Compared with the conventional PTC technique, the key differences are those blocks about candidate voltage vectors that have been colored green. With the proposed DB-PTC with DSVM technique, only three voltage vectors are tested. However, in the conventional PTC technique, all voltage vectors are enumerated.

V. Experiment Evaluation

The test bench is shown in Fig. 7. The dSPACE platform (DS1103) is used in this experiment. In the proposed DB-PTC with DSVM technique, one sampling period subdivided into N parts is realized by using a timer interrupt. In the experiment, the conventional PTC method and the proposed method are tested on the same test bench, with the same sampling period of 60 μs, the same PI parameters, and the same cost function.

TABLE I
PARAMETERS OF THE TESTED IPMSM

Rated torque	2 N·m
Rated current/voltage (rms)	50 A/13 V
Number of pole pairs	5
d/q-axis inductance	0.05/0.095 mH
Resistance	18 mΩ
Rated/maximum speed	2000/4000 r/min
The moment of inertia	0.00187 kg·m^2
PM rotor flux linkage	0.00707 Wb

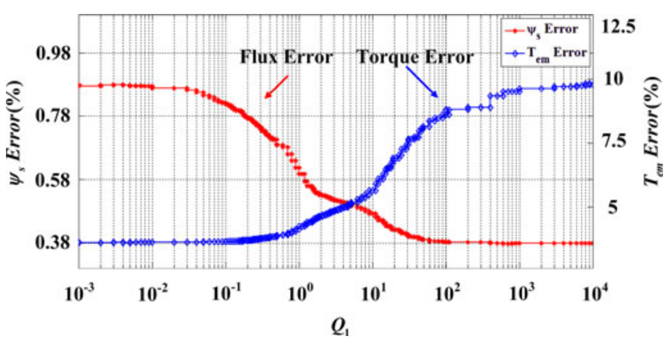

Fig. 8. Average torque error and flux error vary with Q_1.

The machine is a novel designed concentrated windings interior permanent magnet synchronous motor (IPMSM) [38]; the parameters of the motor are shown in Table I. The rated parameters of the motor are served as base values per unit system.

A. Weighting Factor Selection

In this experiment, the motor speed is 0.05 p.u. (100 r/min) and the load torque is 0.2 p.u. (0.4 N·m). One sampling period is subdivided into three parts equally.

In the first step, only torque and flux are considered to select Q_1. Q_1 varies from 10^{-3} to 10^4; the experimental results are shown in Fig. 8. The torque error and the flux error are calculated based on (19) and (20), respectively,

$$T_{\text{error}} = \frac{1}{T_{\text{ref}}}|T_{\text{ref}} - T_e| \tag{19}$$

$$\psi_{\text{error}} = \frac{1}{\psi_{\text{ref}}}|\psi_{\text{ref}} - |\psi_s||. \tag{20}$$

At the intersection of the two curves, low torque error and flux error can be achieved, so 5.2 is chosen for Q_1.

The second step is to select a proper value for Q_2. Q_2 varies from 10^{-7} to 10^0; the torque error and the flux error are shown in Fig. 9.

It can be seen from Fig. 9 that the torque error and the flux error have a similar variation trend. The flux error and the switching frequency are shown in Fig. 10. As DB-PTC with DSVM is a variable switching frequency method, for every Q_2, the switching frequency is nonconstant.

Torque and flux are the two most important control objects. In order to achieve low torque error, low flux error, and low switching frequency, 2×10^{-4} is chosen for Q_2.

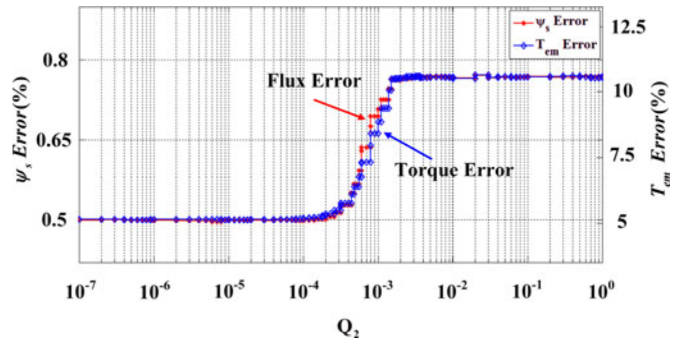

Fig. 9. Average torque error and flux error vary with Q_2.

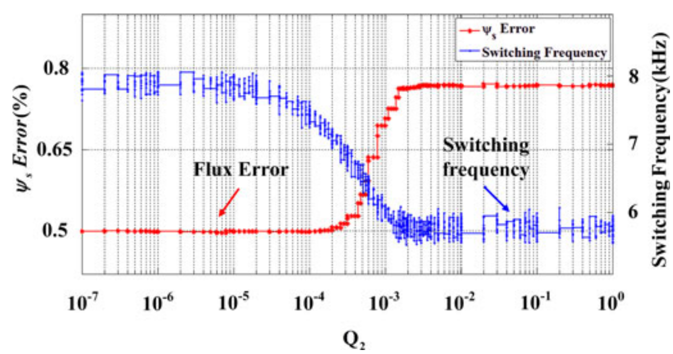

Fig. 10. Flux error and average switching frequency vary with Q_2.

TABLE II
TURNAROUND TIME COMPARISON BETWEEN THE CONVENTIONAL PTC TECHNIQUE AND THE DB-PTC WITH DSVM STRATEGY

Multistep prediction	One step		Two steps	
Strategy	PTC	PTC-DSVM	PTC	PTC-DSVM
Time [μs]	24.58	24.42	85.73	44.25
Tested voltage vectors	7	3	49	9
Time reduction [%]	0.65		48.38	

When Q_1 is 5.2, Q_2 is 2×10^{-4}, the speed is 100 r/min, and the load torque is 0.4 N·m. The torque error is 5.2%, the flux error is 0.5%, and the average switching frequency is 7.35 kHz.

B. Computation Burden

In order to compare the computation burden of the conventional PTC strategy and the DB-PTC with DSVM strategy, the turnaround time is used as a criterion, which can be read directly on the control desk. The turnaround time includes the communication time between dSPACE and control desk, A/D and D/A conversion time, and code implementation time and data saving time. The turnaround time of the two strategies is shown in Table II. "PTC" represents the conventional PTC method, and "PTC-DSVM" denotes the DB-PTC with DSVM strategy.

It can be seen that in one-step prediction, the turnaround time of the two methods is almost the same. However, in long horizon prediction, the computation burden of the proposed technique is significantly lower.

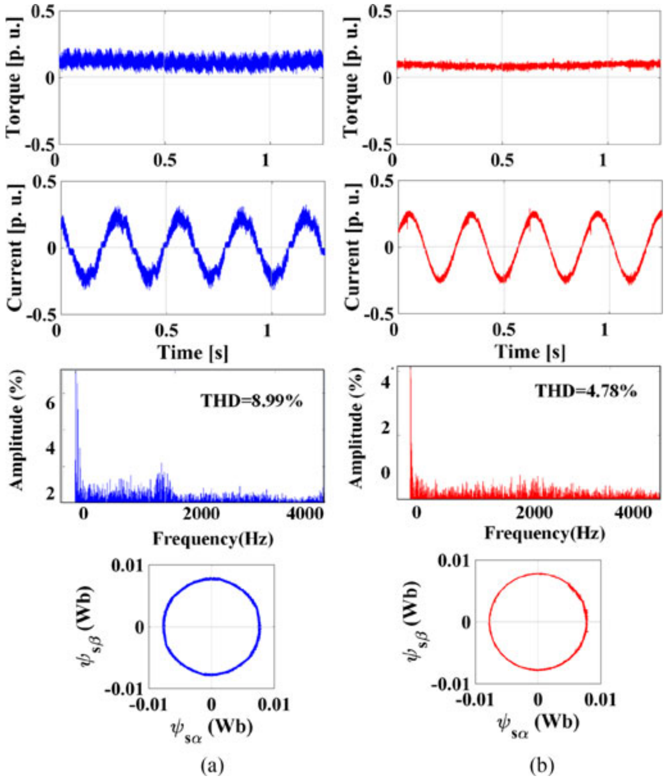

Fig. 11. Steady-state performance comparison at 100 r/min (0.05 p.u.). (a) Conventional PTC technique. (b) DB-PTC with DSVM technique.

No matter how many parts one sampling period is subdivided into, as only three voltage vectors are tested, the computation time of the proposed method is always the same.

C. Steady-State Performance Comparison Between Conventional PTC and DB-PTC With DSVM Methods

This test is used to compare the steady-state performance of the DB-PTC with DSVM technique and the conventional PTC method. In the DB-PTC with DSVM method, one sampling period is subdivided into three parts. The load torque is 0.4 N·m (0.2 p.u.) and the speed is $n = 100$ r/min (0.05 p.u.). The torque waveform, the current waveform, the current total harmonic distortion (THD), and the stator flux linkage are shown in Fig. 11.

In order to get a more convincing conclusion, from 100 r/min (0.05 p.u.) to 2000 r/min (1 p.u.), the current THD and switching frequency comparison of the two methods is shown in Fig. 12.

It can be seen that in the whole speed range, the current THD of the proposed DB-PTC with DSVM technique is obviously smaller.

In order to compare the two methods under the same switching frequency, the switching frequency of the conventional PTC method is used as a reference, by modifying sampling period of the proposed method to achieve an approximate value.

At 100 r/min, the experimental results are shown in Table III. The current THD of the proposed method is 51.35% of the conventional PTC method.

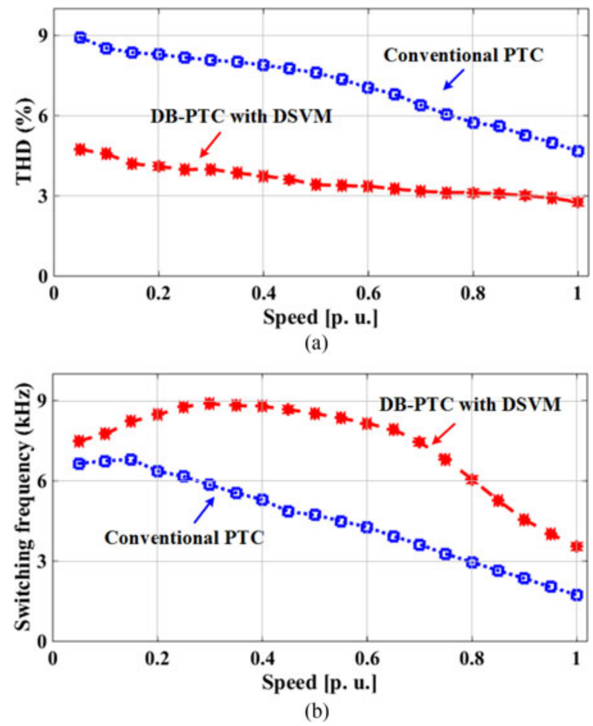

Fig. 12. Steady-state comparison of the conventional PTC technique and the DB-PTC with DSVM technique. (a) Current THD comparison. (b) Switching frequency comparison.

TABLE III
STEADY-STATE PERFORMANCE COMPARISON UNDER THE SAME SWITCHING FREQUENCY

Sampling period		Switching frequency		THD	
μs		Hz		%	
PTC	PTC-DSVM	PTC	PTC-DSVM	PTC	PTC-DSVM
60	63	6975	6940	8.92	4.58

D. Speed Reference Step Change

This experiment is developed for the wide speed range operation. The speed command changes from positive 2000 r/min (1 p.u.) to negative 2000 r/min (-1 p.u.). The electromagnetic torque, the mechanical speed, and the stator phase current are shown in Fig. 13.

It can be seen that from positive 2000 r/min (1 p.u.) to negative 2000 r/min (-1 p.u.), the dynamic performance of the two methods is almost the same.

E. Number of Virtual Voltage Vectors

If one sampling period is subdivided into N parts, with the increase of N, the current THD and the switching frequency of the proposed method are shown in Fig. 14. The load torque is 0.4 N·m (0.2 p.u.) and the speed is $n = 100$ r/min (0.05 p.u.).

It can be seen that with the increase of N, the current THD of the proposed method reduces and the switching frequency increases. In order to achieve a proper N, a good solution

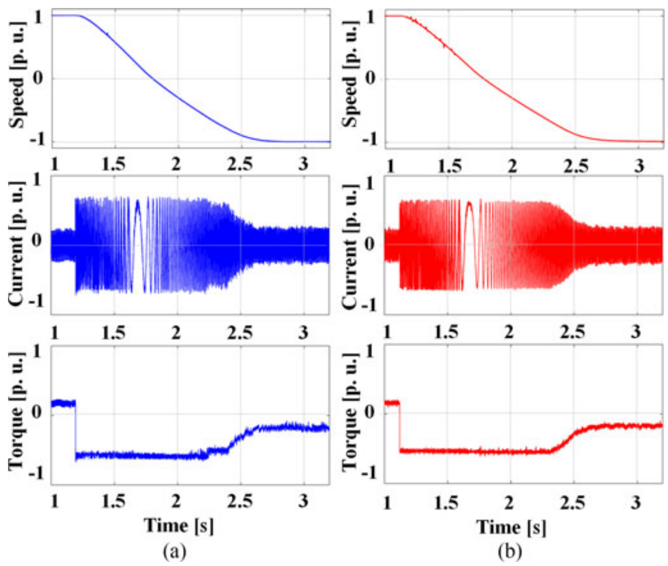

Fig. 13. Experimental results for reference speed changing from 2000 r/min (1 p.u.) to −2000 r/min (−1 p.u.). (a) Conventional PTC method. (b) DB-PTC with DSVM method.

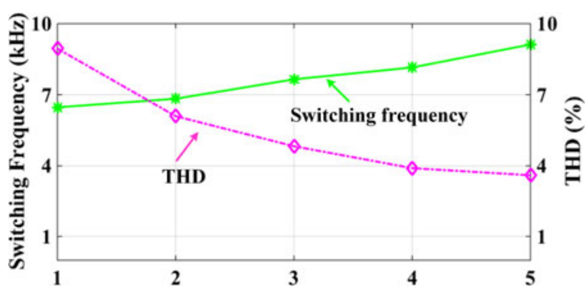

Fig. 14. Current THD and switching frequency change with N.

should be defined as a compromise between the current THD and the switching frequency. It is obvious that with the proposed method, the switching frequency decouples with the sampling time.

F. Steady-State Performance Comparison Between DB-DTFC and DB-PTC With DSVM Methods

In the proposed strategy, DB-DFTC is used to calculate the DB-VV. Generally, the DB-VV is output by using a standard space vector modulator (SVM) [32], [33]. Therefore, it is essential to compare the performance between the DB-DTFC with standard SVM and the DB-PTC with DSVM method. In order to make sure that the selected voltage vector is close to the DB-VV, in the DB-PTC with DSVM method, one sampling period is subdivided into five parts.

From 100 r/min (0.05 p.u.) to 2000 r/min (1 p.u.), the current THD comparison of the two methods is shown in Fig. 15. The two methods are compared under the same switching frequency.

Under the same switching frequency, the current THD of the two methods is almost the same. But the proposed method has the merits of the PTC method, which applies the switching signals to the inverter directly, and the external modulator is

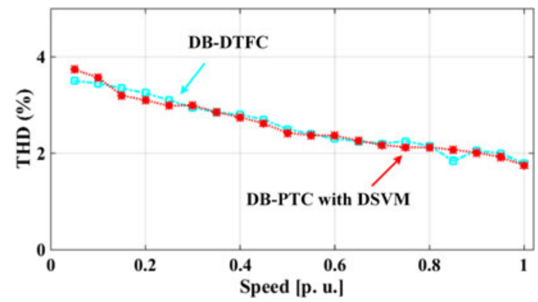

Fig. 15. Steady-state comparison of the DB-DTFC technique and the DB-PTC with DSVM technique.

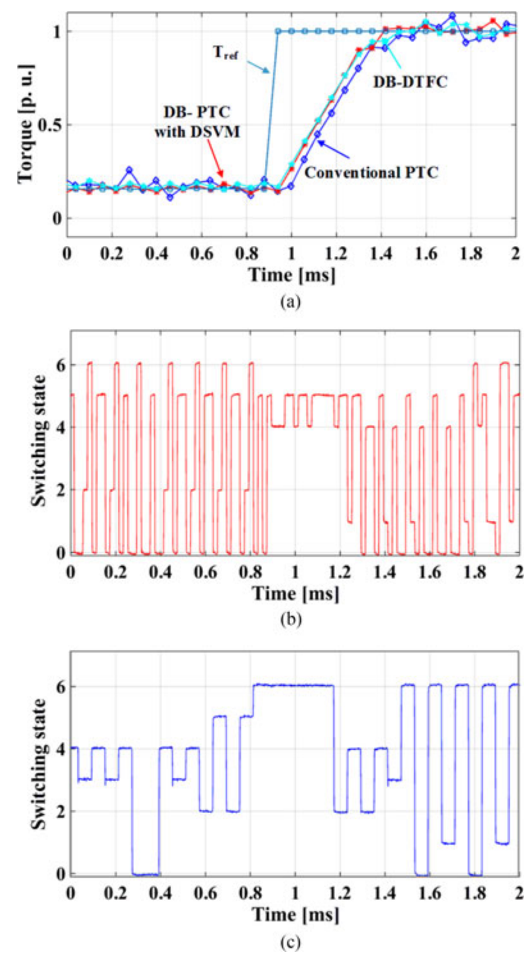

Fig. 16. One-step torque response and the switching states comparison. (a) One-step torque response comparison. (b) Switching state variation of the DB-PTC with DSVM technique. (c) Switching states variation of the conventional PTC technique.

not required. Meanwhile, constraints and nonlinearities can be included, and continuous control set can be considered.

G. Dynamic Response Evaluation

This test is used to compare the dynamic response of the conventional PTC method, the DB-PTC with DSVM method, and the DB-DTFC with standard SVM method. Fig. 16 shows a step change of torque command. The command torque step is limited to a feasible value of 2 N·m (1 p.u.), which is generated by a sudden speed change, from 200 r/min (0.1 p.u.) to 2000 r/min (1 p.u.). Fig. 16(a) shows the torque variation of the three methods. Fig. 16(b) and (c) shows the switching states of the inverter. The switching state "0" means "000,"..., "6" means "110".

Obviously, the torque response of the DB-PTC with DSVM method is faster than that of the conventional PTC method. In both methods, before and after the torque step, the switching states are selected among the zero state (0) and active states (1 to 6). During the torque step, only active states are selected. The torque responses of the DB-DTFC method and the proposed method are almost the same.

VI. Conclusion

Compared with the conventional PTC strategy, the proposed method has many benefits: computation time is shorter, the current THD and torque ripple are lower, the step torque response is faster, and the switching frequency is decoupled with the sampling time. Additionally, the proposed method can track the command speed variation very well.

Compared with the DB-DTFC method, the current THD of the proposed method is almost the same. But the proposed method has the merits of the PTC method at the same time. On one hand, the switching signals are applied to the inverter directly, and the external modulator is not required. On the other hand, constraints and nonlinearities can be included, and continuous control set can be considered.

With the increase of feasible voltage vectors, the current THD of the proposed method is lower and the switching frequency is higher. Meanwhile, the three candidate voltage vectors will be closer to the DB-VV. However, no matter how many voltage vectors are synthesized, only three voltage vectors are tested in each step; thus, the calculation time is the same. In order to achieve a proper number of feasible voltage vectors, a good solution should be defined as a compromise between the current THD and the switching frequency.

References

[1] T. Geyer, G. A. Beccuti, G. Papafotiou, and M. Morari, "Model predictive direct torque control of permanent magnet synchronous motors," in *Proc. IEEE Energy Convers. Congr. Expo.*, Sep. 2010, pp. 199–206, doi: 10/1109/ECCE.2010.5618044.

[2] J. Rodriguez, R. M. Kennel, J. R. Espinoza, M. Trincado, C. A. Silva, and C. A. Rojas, "High-performance control strategies for electrical drives: An experimental assessment," *IEEE Trans. Ind. Electron.*, vol. 59, no. 2, pp. 812–820, Jun. 2012, doi: 10/1109/TIE.2011.2158778.

[3] S. Kouro, P. Cortes, R. Vargas, U. Ammann, and J. Rodriguez, "Model predictive control—A simple and powerful method to control power converters," *IEEE Trans. Ind. Electron.*, vol. 56, no. 6, pp. 1826–1838, Jun. 2009, doi: 10/1109/TIE.2008.2008349.

[4] G. Cimini, D. Bernardini, A. Bemporad, and S. Levijoki, "Online model predictive torque control for permanent magnet synchronous motors," in *Proc. IEEE Int. Conf. Ind. Technol.*, Jun. 2015, pp. 2308–2313, doi: 10/1109/CIT.2015.7125438.

[5] P. Cortes, M. P. Kazmierkowski, R. M. Kennel, D. E. Quevedo, and J. Rodriguez, "Predictive control in power electronics and drives," *IEEE Trans. Ind. Electron.*, vol. 55, no. 12, pp. 4312–4324, Dec. 2008, doi: 10/1109/TIE.2008.2007480.

[6] K. Sangshin and P. Jun-Cheol, "Switching strategy based on model predictive control of VSI to obtain high efficiency and balanced loss distribution," *IEEE Trans. Power Electron.*, vol. 29, no. 9, pp. 4551–4567, Sep. 2014, doi: 10/1109/TPEL.2013.2286407.

[7] S. Vazquez *et al.*, "Model predictive control: A review of its applications in power electronics," *IEEE Ind. Electron. Mag.*, vol. 8, no. 1, pp. 16–31, Mar. 2014, doi: 10/1109/MIE.2013.2290138.

[8] J. Bocker, B. Freudenberg, A. The, and S. Dieckerhoff, "Experimental comparison of model predictive control and cascaded control of the modular multilevel converter," *IEEE Trans. Power Electron.*, vol. 30, no. 1, pp. 422–430, Jan. 2015, doi: 10/1109/TPEL.2014.2309438.

[9] S. Vazquez *et al.*, "Model predictive control with constant switching frequency using a discrete space vector modulation with virtual state vectors," in *Proc. IEEE Int. Conf. Ind. Technol.*, Feb. 2009, pp. 1–6, doi: 10/1109/ICIT.2009.4939728.

[10] L. Tarisciotti, P. Zanchetta, A. Watson, S. Bifaretti, and J. C. Clare, "Modulated model predictive control for a seven-level cascaded H-bridge back-to-back converter," *IEEE Trans. Ind. Electron.*, vol. 61, no. 10, pp. 5375–5383, Oct. 2014, doi: 10/1109/TIE.2014.2300056.

[11] P. Karamanakos, P. Stolze, R. M. Kennel, S. Manias, and H. du Toit Mouton, "Variable switching point predictive torque control of induction machines," *IEEE J. Emerg. Sel. Topics Power Electron.*, vol. 2, no. 2, pp. 285–295, Jun. 2014, doi: 10/1109/JESTPE.2013.2296794.

[12] T. Geyer and D. E. Quevedo, "Multistep finite control set model predictive control for power electronics," *IEEE Trans. Power Electron.*, vol. 29, no. 12, pp. 6836–6846, Dec. 2014, doi: 10/1109/TPEL.2014.2306939.

[13] P. Stolze, M. Tomlinson, R. Kennel, and T. Mouton, "Heuristic finite-set model predictive current control for induction machines," in *Proc. IEEE ECCE Asia Downunder*, Aug. 2013, pp. 1221–1226, doi: 10/1109/ECCE-Asia.2013.6579264.

[14] X. Wei *et al.*, "Finite-control-set model predictive torque control with a deadbeat solution for PMSM drives," *IEEE Trans. Ind. Electron.*, vol. 62, no. 9, pp. 5402–5410, Sep. 2015, doi: 10/1109/TIE.20152410767.

[15] R. Kennel and A. Linder, "Generalized predictive control (GPC)—Ready for use in drive applications?" in *Proc. 32nd Annu. IEEE Power Electron. Spec. Conf.*, Aug. 2002, vol. 4, pp. 1839–1844, doi: 10/1109/PESC.2001.954389.

[16] A. Bemporad, M. Morari, V. Dua, and E. N. Pistikopoulos, "The explicit linear quadratic regulator for constrained systems," *Automatica*, vol. 38, no. 1, pp. 3–20, Oct. 2001, doi: 10/1016/S0005.10980100174.1.

[17] J. Raath, D. T. Mouton, and T. Geyer, "Integration of inverter constraints in geometrical quantification of the optimal solution to an MPC controller," in *Proc. IEEE 17th Workshop Control Model. Power Electron.*, Jun. 2016, pp. 1–6, doi: 10/1109/COMPEL2016.7556711.

[18] M. Preindl, S. Bolognani, and C. Danielson, "Model predictive torque control with PWM using fast gradient method," in *Proc. 28th Annu. IEEE Appl. Power Electron. Conf. Expo.*, Mar. 2013, pp. 2590–2597, doi: 10/1109/APEC.2013.6520661.

[19] D. Casadei, G. Serra, and A. Tani, "Implementation of a direct control algorithm for induction motors based on discrete space vector modulation," *IEEE Trans. Power Electron.*, vol. 15, no. 4, pp. 769–777, Jul. 2000, doi: 10/1109/63.849048.

[20] T. Geyer and S. Mastellone, "Model predictive direct torque control of a five-level ANPC converter drive system," *IEEE Trans. Ind. Appl.*, vol. 48, no. 5, pp. 1565–1575, Jul./Aug. 2012, doi: 10/1109/TIA.2012.2210174.

[21] C. D. Townsend, T. J. Summers, J. Vodden, A. J. Watson, R. E. Betz, and J. C. Clare, "Optimization of switching losses and capacitor voltage ripple using model predictive control of a cascaded H-bridge multilevel STATCOM," *IEEE Trans. Power Electron.*, vol. 28, no. 7, pp. 3077–3087, Jul. 2013, doi: 10/1109/TPEL.2012.2219593.

[22] R. Gregor *et al.*, "Predictive-space vector PWM current control method for asymmetrical dual three-phase induction motor drives," *IET Elect. Power Appl.*, vol. 4, no. 1, pp. 26–34, Jan. 2010, doi: 10/1049/iet-epa.2008.0274.

[23] T. Geyer, G. Papafotiou, and M. Morari, "Model predictive direct torque control—Part I: Concept, algorithm, and analysis," *IEEE Trans. Ind. Electron.*, vol. 56, no. 6, pp. 1894–1905, Jun. 2009, doi: 10/1109/TIE.2008.2007030.

[24] M. Pacas and J. Weber, "Predictive direct torque control for the PM synchronous machine," *IEEE Trans. Ind. Electron.*, vol. 52, no. 5, pp. 1350–1356, Oct. 2005, doi: 10/1109/TIE.2005.855662.

[25] P. Landsmann, P. Stolze, and R. Kennel, "Optimal switching time calculation in predictive torque control," in *Proc. 8th IEEE Int. Conf. Power Electron. ECCE Asia*, Jul. 2011, pp. 923–930, doi: 10/1109/ICPE.2011.5944645.

[26] E. Flach, R. Hoffmann, and P. Mutschler, "Direct mean torque control of an induction motor," in *Proc. Eur. Conf. Power Electron. Appl.*, Mar. 1997, vol. 3, pp. 3.672–3.677.

[27] S. A. Davari, D. A. Khaburi, and R. Kennel, "An improved FCS-MPC algorithm for an induction motor with an imposed optimized weighting factor," *IEEE Trans. Power Electron.*, vol. 27, no. 3, pp. 1540–1551, Mar. 2012, doi: 10/1109/TPEL.2011.2162343.

[28] P. Landsmann and R. Kennel, "Saliency-based sensorless predictive torque control with reduced torque ripple," *IEEE Trans. Power Electron.*, vol. 27, no. 10, pp. 4311–4320, Oct. 2012, doi: 10/1109/TPEL.2012.2192137.

[29] X. Wei, D. Chen, and C. Zhao, "Minimization of torque ripple of direct-torque controlled induction machines by improved discrete space vector modulation," *Elect. Power Syst. Res.*, vol. 72, no. 2, pp. 103–112, Jun. 2004, doi: 10/1016/j.epsr.2004.03004.

[30] J. Villegas, S. Vazquez, J. M. Carrasco, and I. Gil, "Model predictive control of a switched reluctance machine using discrete space vector modulation," in *Proc. IEEE Int. Symp. Ind. Electron.*, Jul. 2010, pp. 3139–3144, doi: 10/1109/ISIE.2010.5637881.

[31] M. Preindl and S. Bolognani, "Model predictive direct speed control with finite control set of PMSM drive systems," *IEEE Trans. Power Electron.*, vol. 28, no. 2, pp. 1007–1015, Feb. 2013, doi: 10/1109/TPEL.2012.2204277.

[32] L. Jae Suk, C. Chan-Hee, S. Jul-Ki, and R. D. Lorenz, "Deadbeat-direct torque and flux control of interior permanent magnet synchronous machines with discrete time stator current and stator flux linkage observer," *IEEE Trans. Ind. Appl.*, vol. 47, no. 4, pp. 1749–1758, May/Jun. 2011, doi: 10/1109/TIA.2011.2154293.

[33] R. D. Lorenz, "The emerging role of dead-beat, direct torque and flux control in the future of induction machine drives," in *Proc. 11th Int. Conf. Optim. Elect. Electron. Equip.*, May 2008, pp. XIX–XXVII, doi: 10/1109/OPTIM.2008.4602331.

[34] P. Cortes *et al.*, "Guidelines for weighting factors design in model predictive control of power converters and drives," in *Proc. IEEE Int. Conf. Ind. Technol.*, May 2009, pp. 1–7, doi: 10/1109/ICIT.2009.4939742.

[35] W. Fengxiang, C. Zhe, P. Stolze, J. F. Stumper, J. Rodriguez, and R. Kennel, "Encoderless finite-state predictive torque control for induction machine with a compensated MRAS," *IEEE Trans. Ind. Informat.*, vol. 10, no. 2, pp. 1097–1106, May 2014, doi: 10/1109/TII.2013.2287395.

[36] W. Xie, X. Wang, F. Wang, W. Xu, R. Kennel, and D. Gerling, "Dynamic loss minimization of finite control set-model predictive torque control for electric drive system," *IEEE Trans. Power Electron.*, vol. 31, no. 1, pp. 849–860, Jan. 2016, doi: 10/1109/TPEL.2015.2410427.

[37] Z. Hao, X. Xi, and L. Yongdong, "Torque ripple reduction of the torque predictive control scheme for permanent-magnet synchronous motors," *IEEE Trans. Ind. Electron.*, vol. 59, no. 2, pp. 871–877, Feb. 2012, doi: 10/1109/TIE.2011.2157278.

[38] W. Xiaocan, X. Wei, G. Dajaku, R. M. Kennel, D. Gerling, and R. D. Lorenz, "Position self-sensing evaluation of novel CW-IPMSMs with an HF injection method," *IEEE Trans. Ind. Appl.*, vol. 50, no. 5, pp. 3325–3334, Sep./Oct. 2014, doi: 10/1109/TIA.2014.2311507.

Yuanlin Wang (S'16) was born in Shaanxi, China, in 1988. He received the B.S. and M.S. degrees in electrical engineering in 2011 and 2014, respectively, from Northwestern Polytechnical University, Xi'an, China, where he is working toward the Ph.D. degree.

He is currently a Visiting Ph.D. Student with the Institute for Electrical Drives and Actuators, Universitaet der Bundeswehr Muenchen, Munich, Germany. His research interests include advanced control for electrical drives and machine design.

Xiaocan Wang (S'13–M'14) was born in Henan, China, in 1984. She received the master's degree in electrical engineering from Northwestern Polytechnical University, Xi'an, China, in 2010, and the Ph.D. degree in electrical engineering from the Institute for Electrical Drive Systems and Power Electronics, Technische Universitaet Muenchen, Munich, Germany, in 2015.

She has been a Senior Development Engineer with Dong Ming Motor Electric Europe GmbH, Munich, since 2015. Her research interests include predictive control and sensorless control for synchronous machines.

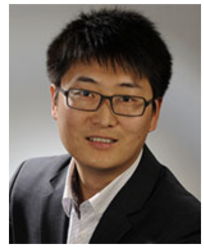

Wei Xie (S'13–M'14) was born in Inner Mongolia, China, in 1982. He received the master's degree in electrical engineering from Northwestern Polytechnical University, Xi'an, China, in 2011, and the Ph.D. degree in electrical drives and actuators from the Universitaet der Bundeswehr Muenchen, Munich, Germany, in 2015.

In 2015, he joined Hitachi Automotive Systems Europe GmbH, Oberding, Germany, where he is a System Engineer working in the field of electric vehicles. He also works with VOLABO, Munich. His research interests include predictive control and sensorless control for electrical drives.

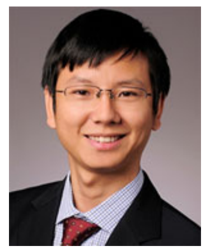

Fengxiang Wang (S'13–M'14) was born in Jiujiang, China, in 1982. He received the B.S. degree in electronic engineering and the M.S. degree in automation from Nanchang Hangkong University, Nanchang, China, in 2005 and 2008, respectively, and the Ph.D. degree in electrical engineering from the Institute for Electrical Drive Systems and Power Electronics, Technische Universitaet Muenchen, Munich, Germany, in 2014.

He is currently with Haixi Institutes, Chinese Academy of Sciences, Jinjiang, China. His research interests include predictive control and sensorless control for electrical drives.

Manfeng Dou (M'08) was born in China in 1967. He received the M.S. and Ph.D. degrees in electrical engineering from Northwestern Polytechnical University (NPU), Xi'an, China, in 1991 and 1998, respectively.

He is a Professor with NPU. He is also the Vice Director of the Institute of Rare Earth Permanent Magnet Electric Machine and Control Technology, NPU. His research interests include electrical machine design, analysis of electromagnetic fields, motion control technology, and intelligent control.

Ralph M. Kennel (M'89–SM'96) was born in Kaiserslautern, Germany, in 1955. He received the Diploma and Dr.-Ing. (Ph.D.) degrees in electrical engineering from the University of Kaiserslautern, Kaiserslautern, in 1979 and 1984, respectively.

From 1994 to 1999, he was a Visiting Professor at Newcastle University, Newcastle upon Tyne, U.K. From 1999 to 2008, he was a Professor in electrical machines and drives at the University of Wuppertal, Wuppertal, Germany. Since 2008, he has been a Professor of electrical drive systems and power electronics at the Technische Universtaet Muenchen, Munich, Germany. His main research interests include sensorless control of ac drives, predictive control of power electronics, and hardware-in-the-loop systems.

Prof. Kennel is a Fellow of the Institution of Engineering and Technology, U.K., and a Chartered Engineer in the U.K. Within IEEE, he is a Treasurer of the Germany Section as well as ECCE Global Partnership Chair of the IEEE Power Electronics Society.

Robert D. Lorenz (S'83–M'84–SM'91–F'98) received the B.S. degree in electromechanical engineering, the M.S. degree in adaptive control, and the Ph.D. degree in electro-optical sensing from the University of Wisconsin–Madison, Madison, WI, USA, in 1969, 1970, and 1984, respectively. He received the M.B.A. degree (Executive Development Program) from the University of Rochester, Rochester, NY, USA, in 1980.

Since 1984, he has been a member of the faculty of the University of Wisconsin–Madison, where he is the Mead Witter Foundation Consolidated Papers Professor of Control Engineering in the Department of Mechanical Engineering, and the Co-Director of the Wisconsin Electric Machines and Power Electronics Consortium. Prior to joining the university, he worked for 12 years in industry, in Rochester, NY, principally on high-performance drives and synchronized motion control. He has authored more than 270 published technical papers. He is the holder of 24 patents with seven more pending.

Prof. Lorenz has received 28 IEEE Prize Paper Awards for papers on power electronics, drives, self-sensing, and current regulators.

Dieter Gerling (M'01) was born in 1961. He received the Diploma and Ph.D. degrees in electrical engineering from the Technical University of Aachen, Aachen, Germany, in 1986 and 1992, respectively.

From 1986 to 1999, he was with Philips Research Laboratories, Aachen, as a Research Scientist and later as a Senior Scientist. In 1999, he joined Robert Bosch GmbH, Buehl, Germany, as the Director. Since 2001, he has been a Full Professor at the Universitaet der Bundeswehr Muenchen, Munich, Germany, where he is the Head of the Institute of Electrical Drives.